Journal of CO2 Utilization 105 (2026) 103358

Contents lists available at ScienceDirect

Journal of CO2 Utilization

journal homepage: www.elsevier.com/locate/jcou

Pulsed electrolysis controls copper restructuring via dissolution–redeposition to prolong selective CO_2 reduction to ethylene

Blaž Tomc [a,b,*], Mitja Kostelec [a,b], Matic Plut [a], Primož Šket [c], Matjaž Finšgar [d], Martin Šala [e], Mejrema Nuhanović [a,b], Francisco Ruiz-Zepeda [a,f], Dušan Strmčnik [a], Marjan Bele [a], Nejc Hodnik [a,b,f,*]

[a] Department of Materials Chemistry, National Institute of Chemistry, Ljubljana 1000, Slovenia
[b] University of Nova Gorica, Nova Gorica 5000, Slovenia
[c] Slovenian NMR Centre, National Institute of Chemistry, Ljubljana 1000, Slovenia
[d] Faculty of Chemistry and Chemical Engineering, University of Maribor, Maribor 2000, Slovenia
[e] Department of Analytical Chemistry, National Institute of Chemistry, Ljubljana 1000, Slovenia
[f] Institute of Metals and Technology, Ljubljana 1000, Slovenia

ARTICLE INFO

Keywords:
Electrochemical CO_2 reduction
Dissolution-redeposition
Pulsed
Stability
Restructuring

ABSTRACT

Pulsed electrolysis is known to enhance the stability of electrochemical CO_2 reduction (ECO_2R) on copper, yet the mechanistic origin of this effect remains poorly understood. Using identical-location electron microscopy in combination with operando impedance spectroscopy, we show that pulsed operation induces continuous and dynamic restructuring of the copper surface. Over 23 h of electrolysis, the catalyst evolved from its initial morphology into a grain-like architecture decorated with dendritic features enriched in high-index facets. This structural evolution was accompanied by a steady increase in the ethylene-to-hydrogen selectivity ratio. Quantitative analysis of the electrolyte during pulsed electrolysis revealed an approximately 30-fold increase in dissolved copper species compared to static operation, identifying redirected dissolution–redeposition of copper as the central mechanistic pathway by which pulsing governs morphology evolution and, consequently, ECO_2R selectivity.

The limited stability of electrochemical CO_2 reduction (ECO_2R) remains a major bottleneck for industrial implementation [1], with copper-based catalysts being both the most promising [2] and the most problematic [3,4]. During ECO_2R, copper undergoes continuous restructuring [5–25], mainly by dissolution–redeposition [9,14,26,27], which alters both activity and selectivity, typically leading to a gradual loss of the desired product formation [5–13,28–41]. Although recent advances have demonstrated stable operation of >100 h [33,42–44], this is still far from the $>50{,}000$ h required for commercial viability [45], highlighting the urgency of addressing the intrinsic morphological instability of copper [3].

Pulsed ECO_2R is a promising strategy for extending the lifetime of copper catalysts [38,46–50], with reports showing stability improvements by several orders of magnitude [12,13,34–37,50–54]. The approach periodically interrupts the reductive bias with a lower overpotential, dynamically modulating the electrode–electrolyte interfacial equilibria [47,48,55]. Since no special synthesis or electrolyte is required, pulsed operation provides a straightforward route to prolong the ECO_2R [47,48,56,57]. Yet, despite its broad appeal, the mechanistic origin of the performance enhancement remains unclear [47]. Among proposed explanations [47], experimental observations also report that pulsed electrolysis reshapes copper morphology during ECO_2R [13,36,40,50,51,55,58–62]. Since surface structure critically determines selectivity and activity in ECO_2R [42,63–66], it is plausible that pulses prolong operational stability by dynamically redirecting the evolution of copper morphology. This arises from the fact that pulse potentials usually oscillate between the copper oxidation and reduction regimes [12,47,61,62], initiating an oxidation–reduction–driven cycle of dissolution-redeposition [9,67–70]. This dissolution-redeposition pathway importantly differs from the one dominating under solely a reductive bias: (i) reductive dissolution is proposed to occur via the complexation of copper with ECO_2R intermediates [26], whereas oxidative dissolution is expected according to the Pourbaix diagram [9,71], (ii) reductive dissolution occurs in the range of 10-ppb [9,34], while

* Corresponding authors at: Department of Materials Chemistry, National Institute of Chemistry, Ljubljana 1000, Slovenia.
E-mail addresses: blaz.tomc@ki.si (B. Tomc), nejc.hodnik@ki.si (N. Hodnik).

https://doi.org/10.1016/j.jcou.2026.103358
Received 9 October 2025; Received in revised form 28 January 2026; Accepted 8 February 2026
Available online 16 February 2026

oxidative dissolution exceeds 100 ppb [9,68,71], and (iii) redeposition under constant reductive bias occurs at the applied potential on an intermediate-covered surface, whereas during pulsing it takes place under a transient potential bias and thus altered surface coverage. Consequently, we hypothesized that pulsed ECO_2R activates a distinct dissolution–redeposition process that counteracts the deactivation pathways of static operation, leading to modified copper morphology and a divergent evolution of catalytic performance.

Furthermore, previous reports showed that variations in pulse parameters can yield distinct copper morphologies, activities, and selectivities [36,40,60], closely resembling those obtained through diverse ECO_2R pretreatment protocols [9,71–73]. The concept also parallels broader electrochemical synthesis strategies in which electrodeposition via potential cycling tailors material morphologies [48], for instance, copper nanocubes [74].

While these insights suggest that pulsing controls copper restructuring via oxidation-reduction dissolution–redeposition to extend catalyst stability, direct evidence of this link has, to the best of our knowledge, remained unresolved in the field. Here, we provide clear experimental proof of controlled copper restructuring during pulsed electrolysis and establish its direct connection to changes in selectivity, activity, and stability, offering a mechanistic foundation for future efforts to extend ECO_2R durability.

To define a baseline, a copper foil (Sigma-Aldrich, 0.25 mm, 99.98 %) was subjected to prolonged ECO_2R at –1.0 V vs. reversible hydrogen electrode (RHE) in static mode (Fig. 1a-c). Liquid products were quantified by nuclear magnetic resonance following the protocol presented in ref. [9], while other experimental parameters were the same as those reported in ref. [34]. Within three hours, both the geometric current density (j_{Geo}) and ethylene selectivity decreased by more than half. Operando electrochemical impedance spectroscopy (EIS) [34] revealed pronounced changes of the catalysts-electrolyte interface (Fig. 1d,e): an increase in charge-transfer resistance (R_{CT}) indicated more sluggish reaction kinetics, while a drop in double-layer capacitance (c_{DL}) revealed a loss of electrochemical surface area (ECSA). Scanning electron microscopy (SEM) images before and after electrolysis showed a pronounced morphological restructuring during this process, dominated by the formation of ~100 nm particles (Fig. 1f). Overall, these results show that performance loss arose from interfacial changes, with copper restructuring being the most apparent cause, resembling the literature presented in the introduction.

To counter the deactivation, we applied pulsed electrolysis consisting of 2s-long oxidative pulses at + 1 mA every 2 min (Fig. 2a). Each pulse drove the potential above 0.6 V vs. RHE, which had previously been identified as optimal for C_{2+} formation over the hydrogen evolution reaction (HER) [60]. Under this operation, ECO_2R stability was maintained for 23 h without loss of C_{2+} selectivity (Fig. 2b) or activity (Fig. 2c). Ethylene Faradaic efficiency (FE) increased fourfold, methane sixfold, ethanol doubled, while n-propanol FE rose slightly (Figure S1). In contrast, the FE for hydrogen, CO, and formic acid decreased by factors of 2, 7, and 5, respectively. Apart from fluctuations, j_{Geo} remained constant over the entire period. The conditions and the evolution of selectivity provided an ideal platform to confirm the hypotheses on the mechanistic basis of pulsed ECO_2R: (i) no performance loss over 23 h with increased selectivity for products characteristic of copper catalysts and a decreased selectivity for products favored on other catalysts, (ii) changes evolving over a long period of time and at different rates, (iii) pulse parameters consistent with those commonly reported, and (iv) a pulse potential greater than 0.6 V vs. RHE, which triggers the oxidation-reduction and dissolution-redeposition of copper.

To confirm the altered morphological evolution, intermittent identical location SEM (IL-SEM) [9,71,75,76] was employed. The

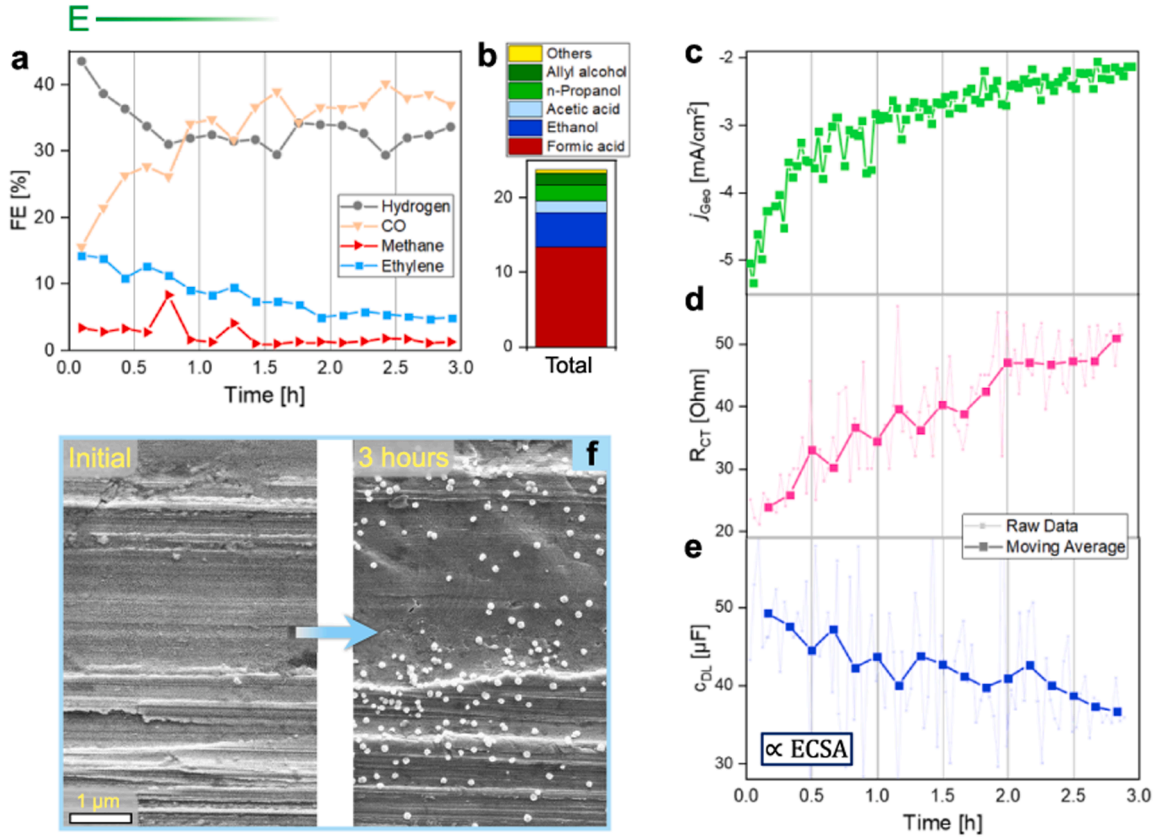

Fig. 1. (a) Evolution of gaseous product selectivity during ECO_2R at a constant potential of –1.0 V vs. RHE with dynamic IR compensation [94] in 0.1 M $KHCO_3$ on copper foil. (b) Selectivity for liquid products over the 3-hour reaction. Time-dependent (c) j_{Geo}, (d) R_{CT}, and (e) c_{DL} (∝ECSA) from operando EIS [34]. (f) SEM images of the copper surface before and after electrolysis.

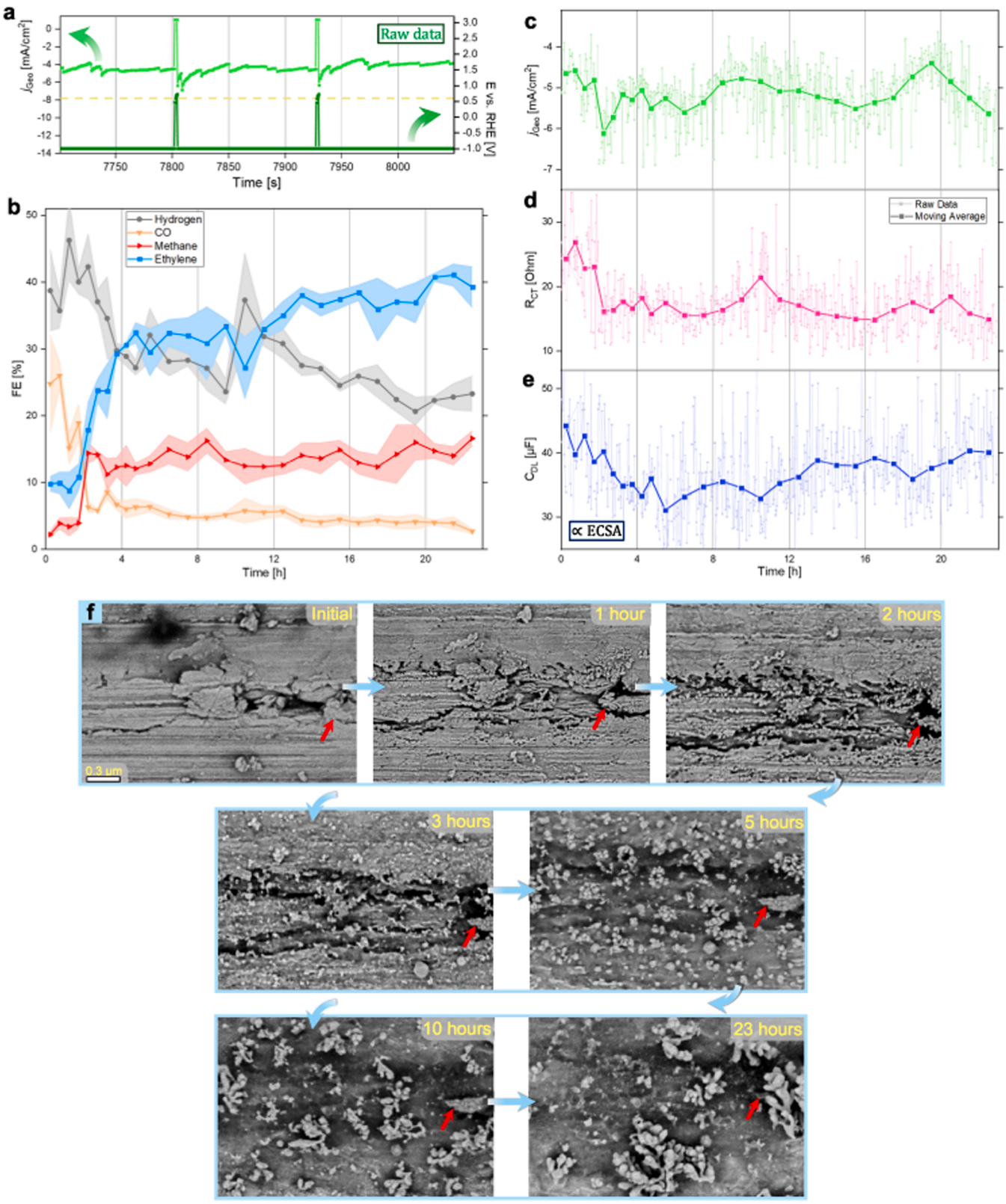

Fig. 2. (a) Applied potential and j_{Geo} during pulsed electrolysis on copper foil; 2 s oxidative pulses at + 1 mA interrupting the −1 V vs. RHE reductive bias every 2 min. The yellow dashed line represents 0.6 V vs. RHE. (b) Time-resolved ECO_2R; shaded regions indicate standard deviations. The evolution of liquid products is provided in Fig. S1. (c) j_{Geo}, (d) R_{CT}, and (e) c_{DL} evolution over 23 h of pulsed operation with operando IR compensation [94] and EIS interface monitoring [34]. (f) IL-SEM images of the copper catalyst at the indicated times. Imaging procedure: electrolyte removal, electrolysis stopped, cell disassembled, sample imaged, cell reassembled, fresh electrolyte introduced, electrolysis restarted. Electrolyte was also exchanged under potential control at hours 7, 9, 12, 14, 17, and 20 to obtain time-resolved liquid product distributions shown in Fig. S1. Images taken with different SEM detectors, magnification, and sample positions are provided in the Supporting Information.

morphological inhomogeneity of copper foil served as markers for repositioning to the same location, while their variability provided a platform to observe how different copper morphologies restructure under the same conditions. Additionally, operando EIS was employed to monitor the changes in the properties of the catalyst-electrolyte interface [34]. As expected, IL-SEM revealed pronounced but gradual changes in the architecture of the catalyst surface, while operando EIS revealed progressive alterations of the interface during operation (Fig. 2d-f). From the data, three interrelated mechanisms could be recognized that reshape copper morphology, interfacial parameters, and selectivity on different time scales, each providing evidence on the proposed mechanism.

Within the first ~2.5 h, R_{CT} decreased by more than 1.5-fold, especially at the end of this period (Fig. 2d), indicating faster reaction kinetics, while c_{DL} dropped slightly (Fig. 2e), reflecting a small loss in ECSA. IL-SEM revealed evident surface modification during this period (Fig. 2f), characterized by the dissolution of exposed features and the emergence of spherical structures in their place (Fig. 3a). Selectivity and activity changed only slightly at first, with pronounced transitions occurring after the 2nd hour, indicating the change of the restructuring mechanism. This initial phase confirmed that copper undergoes active restructuring during pulsed electrolysis; however, it did not yet show any obvious correlations with the ECO_2R selectivity.

Between the ~2nd and ~5th hour, a significant progression in selectivity occurred (Fig. 2b), with the FE for ethylene exceeding the HER FE and reaching 30 %. During this period, R_{CT} remained within experimental error, while c_{DL} decreased (Fig. 2d,e), indicating a decrease in ECSA. IL-SEM showed that the surface gradually became flatter due to the disappearance of polishing scratches (Figures S10 and S11), accompanied by the nucleation and growth of spherical features. These motifs were observed across the whole catalyst exposed to the electrolyte (Figure S14). On average, these changes contribute to the reduction in surface area (Figure S12). Since ECSA reflects the active ECO_2R copper surface area and its decrease paralleled the morphological polishing, this relationship strongly suggests that the evolving ECO_2R selectivity during this period resulted from the evolution of the catalyst surface.

After the second period, the changes in selectivity continued, but at a much slower rate. This indicates that a different mechanism occurred from the ~5th to the ~23rd hour. During this period, the catalyst became even more efficient, reaching a final FE of 40 % for ethylene, while the FE for HER dropped to almost 20 %. Operando EIS showed no discernible drift in R_{CT}, while c_{DL} increased steadily over time. The near-linear increase in ECSA mirrored the linear trends in selectivity of ECO_2R products and HER, indicating a close correlation. IL-SEM showed extensive surface reconstruction (Fig. 2f): the surface developed 3D grain-like features (Figs. 3b, S12, S13, S15, and S16), while copper dendrites gradually formed (Figs. 3c, S13b, and S17). While similar grain-like features were observed across the entire catalyst surface exposed to the electrolyte, larger dendritic structures formed at the bottom of the catalyst, whereas smaller ones were present toward the top (Figure S15). Similar to the correlation between ECSA and

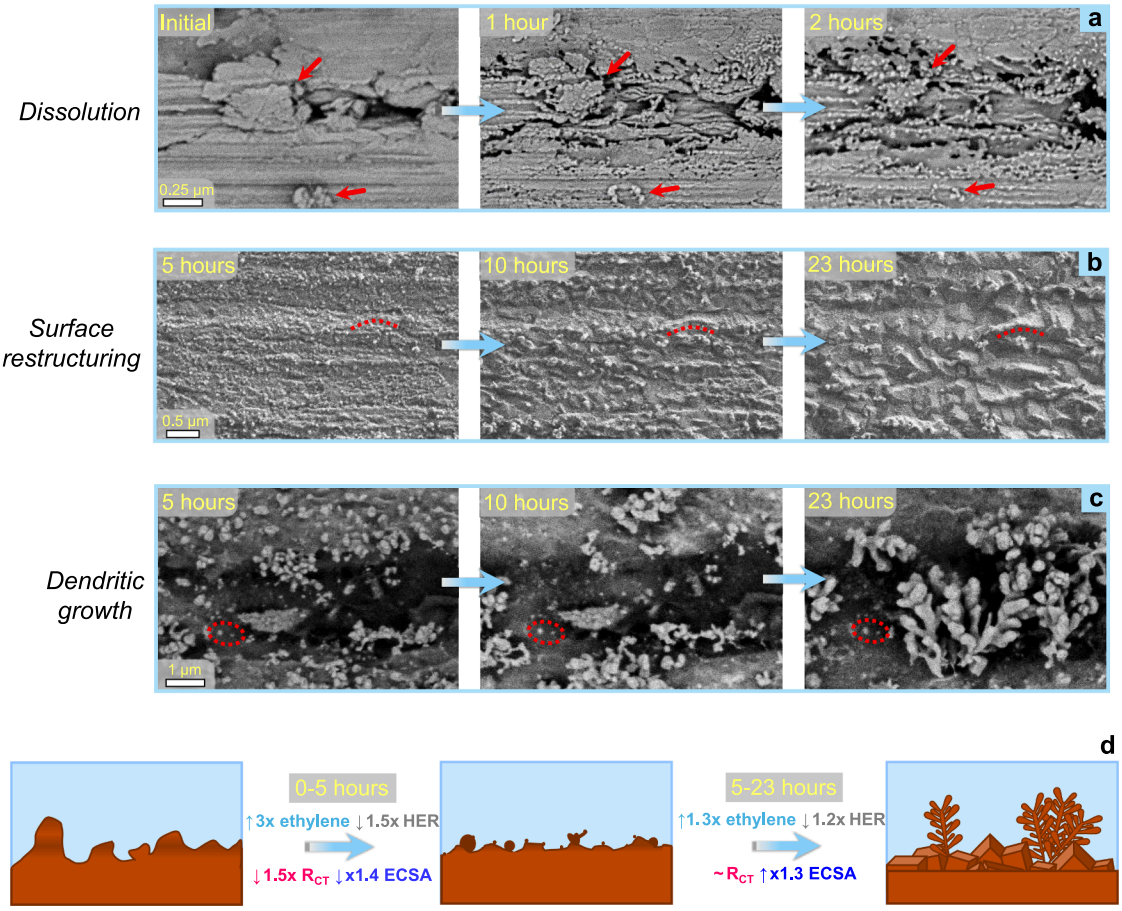

Fig. 3. (a-c) IL-SEM images from Fig. 2 f showing three distinct copper morphology restructuring phenomena occurring at different scales and rates. Red marks denote identifiable features that persist during the pulsed ECO_2R. (d) Schematic representation of these processes over two time periods with corresponding changes in selectivity and reaction parameters.

selectivity, this gradual restructuring of morphology increased the active surface area and mirrored the ECSA trend (Fig. 3d). Together, these two correlations form the morphology-ECSA-ECO_2R selectivity relationship.

The three separate but intertwined mechanisms operating in three different periods therefore support the hypothesis that pulse control over copper surface features is the dominant factor in maintaining ECO_2R selectivity. In the first period, selectivity was likely more constant as surface motifs remained similar through the dissolution of exposed features. In the subsequent period, surface restructuring began to substantially alter the catalyst active sites, resulting in a substantial shift in selectivity. Following the second period, the slow formation of dendrites and a grain-like surface led to a further slight improvement of selectivity for ethylene over HER. Furthermore, by comparing the surface species formed after 3 h of pulsed electrolysis with the ~100 nm particles formed in the constant potential experiment (Figure S18), it is clear that pulses restructure the copper catalyst differently, supporting the hypothesized mechanistic model.

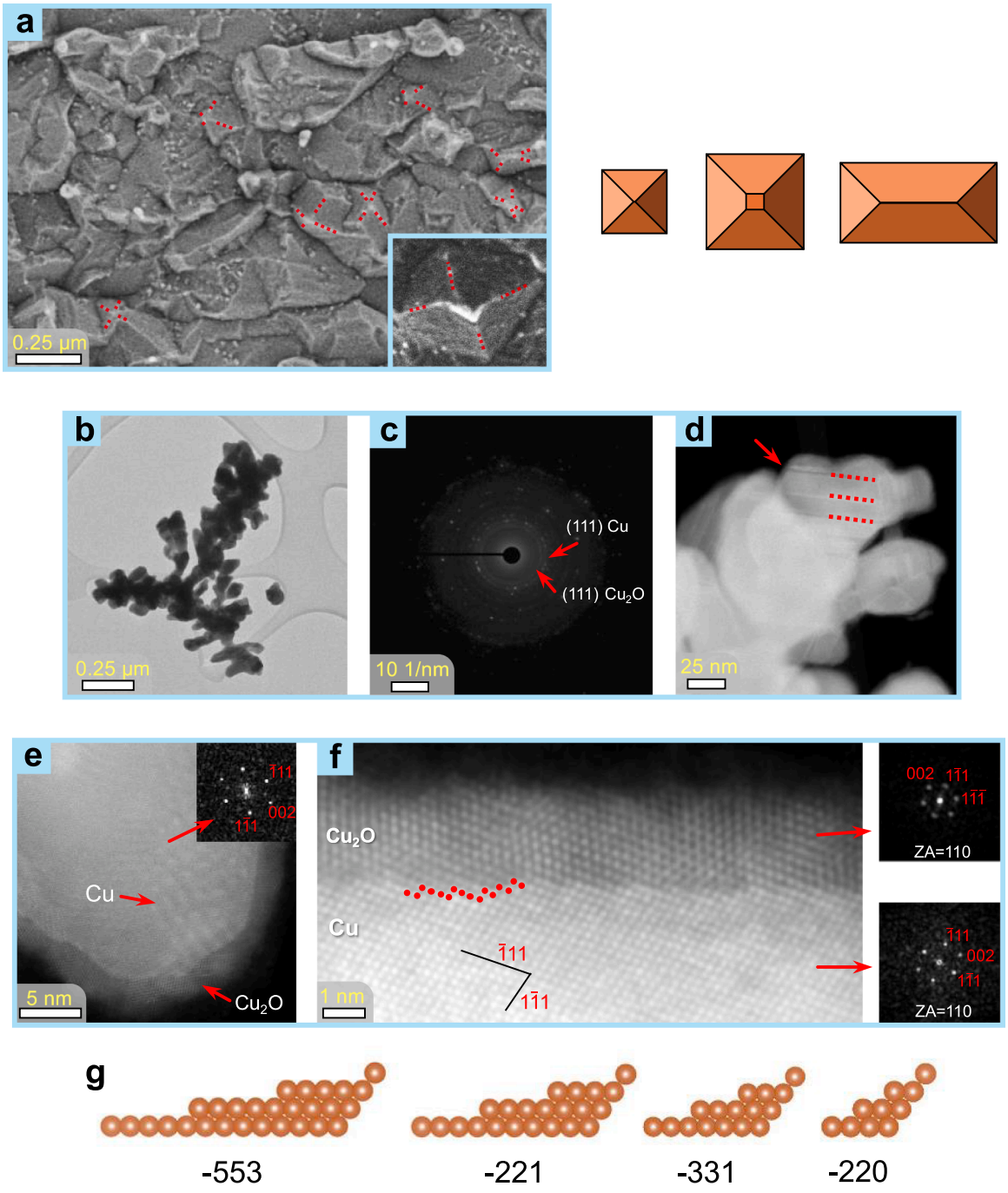

Fig. 4. (a) SEM image of a grain-like surface formed in Fig. 2 experiment, showing a high population of pyramidal features. The image in the bottom right corner showcases a larger pyramid formed at another location. (b) TEM image of a copper dendrite transferred from the Fig. 2 sample onto a TEM grid. (c) SAED ring pattern of a copper dendrite branch, revealing multiple grain formation. (d) ADF image illustrating planar defects along the (111) planes of the copper crystallites that constitute the dendrites. (e) High-resolution ADF image of a copper dendrite branch tip crystallite oriented along the [110] zone axis, displaying Cu and Cu_2O in a core-shell structure. (f) High-resolution ADF image of the surface of a copper dendrite edge with high-index facets visible on the Cu core edge. FFT corresponding to different locations marked by arrows. (g) Atomic models of typical high-index facets observed on the surface.

To understand the enhanced reactivity of the formed surface species after Fig. 2 experiment, the catalyst was additionally analyzed. Upon closer inspection of the grain-like surface, several localized pyramid-like features are observed on the copper catalyst (Fig. 4a). These features are reminiscent of faceting motifs associated with (n10) planes, as recently reported for pulsed ECO_2R on Cu(100) by Tănase et. al. [61]. However, because SEM alone does not allow unambiguous facet assignment, the presence of such (n10)-type facets in the present system can only be hypothesized. On the other hand, the high selectivity is further supported by previous reports identifying copper dendrites as excellent catalysts for ethylene formation [77,78]. To reveal the crystallographic composition of these species, transmission electron microscopy (TEM) and selected area electron diffraction (SAED) were employed by transferring copper dendrites onto a TEM grid.

TEM revealed that the copper dendrites formed under pulsed electrolysis exhibit a complex, defect-rich crystalline architecture rather than a single preferential orientation. A representative dendrite displaying the characteristic fractal morphology [79] is shown in Fig. 4b. SAED patterns acquired from the structure (Fig. 4c) indicate that the dendrites are composed of multiple crystalline grains, consistent with growth governed by repeated dissolution–redeposition events rather than kinetically locked, single-crystal propagation. Annular dark-field (ADF) imaging further revealed the presence of planar defects within individual copper crystallites (Fig. 4d), which can be attributed to growth accidents occurring preferentially along close-packed (111) planes [80].

At the surface of individual dendritic branches, a thin Cu_2O layer was frequently observed, forming a core–shell–like structure atop a metallic Cu core, oriented in the [110] zone axis (Fig. 4e,f). The two distinct phases were confirmed by localized fast Fourier transform (FFT) patterns acquired from the shell and the underlying core. An oxide shell is expected due to unavoidable exposure and subsequent oxidation under ambient conditions, while the growth-entrapped metallic core indicates that the dendrites were predominantly metallic under reductive reaction conditions. Importantly, high-resolution ADF imaging and FFT analysis revealed that the dendrite branch edge surfaces are dominated by high-index facets, most commonly indexed as (−553), (−221), (−331), and (−220), which alternate across the surface (Fig. 4f,g). These facets introduce a heterogeneous coordination environment rich in steps, kinks, and low-coordination copper atoms, providing a plausible structural origin for the enhanced C–C coupling and increased C_{2+} selectivity observed during prolonged pulsed electrolysis [81].

IL-SEM, supported by complementary TEM analysis, revealed two distinct surface structures formed during potential pulsing. To further probe the stability of these structures, the pulsed-electrolysis-prepared sample was subsequently subjected to static electrolysis (Figure S19). Although the decay of ethylene selectivity and the drop in j_{Geo} were temporarily slowed (Figure S19a,b), static operation ultimately failed to sustain favorable ECO_2R efficiency. This observation demonstrates that pulsed electrolysis not only enhances catalytic activity and selectivity but is also required to retain them over extended operation. IL-SEM analysis revealed that the fine dendritic surface structure progressively deteriorated under static electrolysis, breaking down into smaller copper features (Figure S19f), which is in close analogy to degradation pathways previously reported for copper nanoparticles [9]. In contrast, the grain-like surface morphology remained largely preserved (Figure S19e). These observations indicate that pulsed electrolysis induces both quasi-reversible and irreversible restructuring processes. Importantly, this selective degradation strongly suggests that the dendritic structures constitute the most catalytically active sites for C_{2+} formation and that their growth under pulsed electrolysis is the underlying origin of the pronounced selectivity enhancement observed in Fig. 2.

In addition to the morphological restructuring induced by pulsed electrolysis, we also investigated whether this operating regime preserves a significant population of copper oxide species. X-ray photoelectron spectroscopy (XPS) was performed on the sample shown in Fig. 2 after 23 h of pulsed electrolysis. The Cu $L_3M_{4,5}M_{4,5}$ Auger spectra were successfully reproduced by convolution of reference spectra corresponding to Cu(0) and Cu(I) [82], indicating that only these two copper species were present after electrolysis (Figure S20a). Quantitative analysis yielded relative contributions of 62.5 % Cu(0) and 37.5 % Cu(I). For comparison, XPS spectra were recorded for a sample after 15 min of static electrolysis at −1 V vs. RHE. Quantitative analysis yielded relative contributions of 56.7 % from Cu(0) and 43.3 % (Figure S20b). Therefore, in the case example of this study, the pulse regime didn't retain a substantial amount of copper oxides vs. static electrolysis, reinforcing the hypothesis on the controlled copper morphology. However, due to partial copper oxides formation upon air exposure (Fig. 4e,f), operando analysis of copper valence states would need to be performed for the 2 s oxidation 2 min reduction pulse regime used in this study.

As outlined in the Introduction, the observed morphological evolution of the copper surface is underpinned by the physical transport of copper via dissolution–redeposition processes. The hypothesis that pulsed electrolysis operates predominantly through oxidative–reductive dissolution–redeposition is supported by the observation that the morphological features formed under pulsed electrolysis are indistinguishable from those obtained under static electrolysis (Figure S18). This interpretation is further corroborated by the anodic bias applied during the pulses (Fig. 2a), which exceeded 0.6 V vs. RHE—conditions under which copper oxides readily form and dissolve into the electrolyte. Moreover, the emergence of copper dendrites is a characteristic feature of electrodeposition processes [79,83–87].

To experimentally validate this hypothesis, quasi in situ inductively coupled plasma mass spectroscopy (ICP-MS) was employed by sampling aliquots of the electrolyte during electrolysis (Fig. 5a). The experimental protocol was the same as in ref. [71]. Baseline measurements under static electrolysis revealed 6.8 ± 3.7 ppb of dissolved copper species, consistent with previous reports [9,34]. In contrast, electrolyte analysis under pulsed operation showed a substantially higher concentration of dissolved copper (259 ± 61 ppb), indicating a markedly enhanced dissolution–redeposition process compared to static conditions. Notably, dissolved copper concentrations on the order of 100 ppb have previously been associated with oxidative–reductive dissolution–redeposition mechanisms [9,68,71], providing further support for this interpretation.

Additional evidence for pulse-induced copper dissolution was obtained by sampling the electrolyte at different time points within individual pulses (Fig. 5b). An increase in dissolved copper concentration was observed during the oxidative segment of the pulse, reaching a maximum at approximately 10 s of the reductive segment. This behavior indicates dissolution of the oxide layer formed during the anodic phase of the pulse [61]. Beyond the ~10 s mark, a rapid decrease of approximately 100 ppb in dissolved copper concentration was detected, after which the concentration gradually declined with time. Following pulsed operation, the catalyst was held under static electrolysis for 20 min (Fig. 5a), during which the concentration of dissolved copper species continued to decrease. This trend suggests a gradual transition toward a reductive redeposition-dominated regime, in which dissolved copper species are progressively reincorporated onto the catalyst.

Collectively, the results and findings presented here establish the following relationship (Fig. 5c): (i) pulsed electrolysis induces the oxidation-reduction dissolution-redeposition of copper, (ii) this mechanism drives the restructuring of the copper surface in a different direction than under constant conditions, and (iii) the formation of the new surface morphology regulates the ECO_2R selectivity via a structure-performance relationship. Thus, the stability improvements under pulsed conditions are achieved by the redirected dynamics of the copper species. Interestingly, although pulsed electrolysis aimed to stabilize the copper morphology, our results show that it induces even more instability compared to static operation. However, by steering the restructuring in a different direction, C_{2+} favorable copper sites are formed and

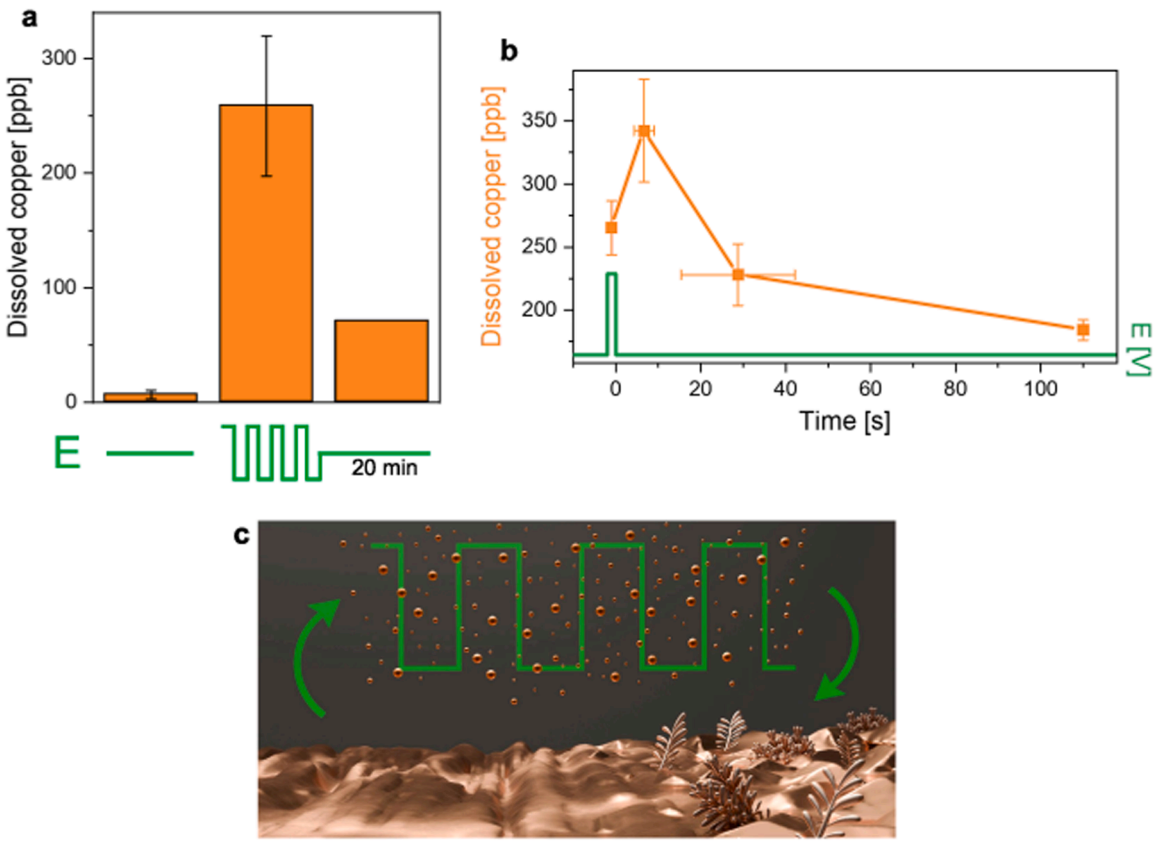

Fig. 5. (a) Dissolved copper quantified by ICP-MS under different electrolysis regimes, as indicated by the potential profiles shown below the plot. For static electrolysis, catholyte samples were collected under potential control from three independent experiments after 15 min, 1 h, and 3 h at a constant potential of −1.0 V vs RHE. For pulsed electrolysis, the catholyte was sampled every two cycles under potential control at defined times within the pulse sequence. After each sampling event, the withdrawn electrolyte volume was immediately replaced with an equal volume of fresh electrolyte. Following 13 measurements acquired over approximately 1 h under pulsed operation, the system was switched to static electrolysis for 20 min, after which the catholyte was sampled again under potential control. (b) Time-resolved copper dissolution was extracted by sampling the electrolyte at distinct moments within the pulse, revealing pulse-dependent dissolution dynamics. (c) Schematic illustration of the dissolution–redeposition mechanism identified in this study.

preserved under the pulse-driven dissolution-redeposition. Therefore, we can refer to this phenomenon as a dynamically stable active copper surface sites, similarly to how it was termed for the oxygen evolution reaction hydr(oxy)oxide surfaces [88,89].

Previous studies have demonstrated that distinct ECO_2R selectivities and catalyst morphologies can be achieved under different pulsed electrolysis regimes, including variations in pulse duration, applied potential, frequency, and waveform of the oxidative and reductive steps [59,60,90]. In our earlier work, we showed that oxidative dissolution is strongly governed by the duration of the open-circuit potential, while variations in the applied reductive bias lead to the development of markedly different copper morphologies [9,71]. Building on these observations, and given that pulsed operation in the present study was shown to proceed via the same underlying principles, we propose that the mechanistic origin of the observed differences in ECO_2R selectivity and morphology under different pulsed regimes arise from pulse-induced modulation of the oxidative–reductive dissolution–redeposition dynamics of copper. Moreover, the knowledge of these redirected copper dynamics under ECO_2R conditions is directly transferable to other copper-catalyzed pulsed electrosynthesis processes, e.g., NH_3 production from NO_3 [91], formaldehyde oxidation [92], etc [93].

In summary, IL-SEM and operando EIS demonstrate that pulsed electrolysis profoundly alters copper morphology during ECO_2R. The observed correlations between surface restructuring, interfacial properties, and selectivity identify redirected catalyst restructuring as the primary effect of electrochemical pulsing. Copper oxidation–reduction dissolution–redeposition is established as the underlying mechanism, whose regulation accounts for the improved stability and the emergence of distinct ECO_2R selectivities. Rather than suppressing catalyst instability, pulsed electrolysis exploits it to steer morphology toward dynamically stable, selective CO_2 reduction. More broadly, these findings highlight dynamic restructuring as a general concept in electrocatalysis.

CRediT authorship contribution statement

Blaž Tomc: Writing – original draft, Visualization, Validation, Project administration, Methodology, Investigation, Data curation, Conceptualization. **Nejc Hodnik:** Writing – review & editing, Validation, Supervision, Funding acquisition. **Matic Plut:** Investigation, Data curation. **Mitja Kostelec:** Visualization, Methodology, Investigation, Data curation. **Matjaž Finšgar:** Investigation, Data curation. **Primož Šket:** Methodology. **Mejrema Nuhanović:** Investigation, Data curation. **Martin Šala:** Investigation, Data curation. **Francisco Ruiz-Zepeda:** Investigation, Data curation. **Marjan Bele:** Validation, Supervision, Methodology, Investigation. **Dušan Strmčnik:** Writing – review & editing, Validation, Supervision.

Declaration of Competing Interest

The authors declare that they have no known competing financial interests or personal relationships that could have appeared to influence the work reported in this paper.

Acknowledgments

The authors would like to acknowledge the Slovenian Research and Innovation Agency (ARIS) through programs P2–0393, P1–0034, P1–0242, I0–0003, and P2–0118; the projects GC-0001, GC-0004, N2–0155, N2–0337, J1–70039, J7–4636, J7–4637, J7–4638, and J7–50227; and European Research Council (ERC) Starting Grant 123STABLE (grant agreement ID: 852208). The project is co-financed by the Republic of Slovenia, the Ministry of Education, Science and Sport, and the European Union under the European Regional Development Fund.

Appendix A. Supporting information

Supplementary data associated with this article can be found in the online version at doi:10.1016/j.jcou.2026.103358.

Data availability

Data will be made available on request.

References

[1] T. Burdyny, Using Pseudo-steady-state operation to redefine stability in CO2 electrolysis, Nat. Chem. Eng. 2 (2025) 350–357.
[2] S. Nitopi, E. Bertheussen, S.B. Scott, X. Liu, A.K. Engstfeld, S. Horch, B. Seger, I.E. L. Stephens, K. Chan, C. Hahn, J.K. Nørskov, T.F. Jaramillo, I. Chorkendorff, Progress and perspectives of electrochemical CO2 reduction on copper in aqueous electrolyte, Chem. Rev. 119 (2019) 7610–7672.
[3] J. Kok, P.P. Albertini, J. Leemans, R. Buonsanti, T. Burdyny, Overcoming copper stability challenges in CO2 electrolysis, Nat. Rev. Mater. 10 (2025) 550–563, https://doi.org/10.1038/s41578-025-00815-0.
[4] S. Popović, M. Smiljanić, P. Jovanovič, J. Vavra, R. Buonsanti, N. Hodnik, Stability and degradation mechanisms of copper-based catalysts for electrochemical CO2 reduction, Angew. Chem. Int. Ed. 59 (2020) 14736–14746.
[5] W. Choi, Y. Chae, E. Liu, D. Kim, W.S. Drisdell, H.S. Oh, J.H. Koh, D.K. Lee, U. Lee, D.H. Won, Exploring the influence of cell configurations on Cu catalyst reconstruction during CO2 electroreduction, Nat. Commun. 15 (2024) 8345.
[6] P. Grosse, D. Gao, F. Scholten, I. Sinev, H. Mistry, B. Roldan Cuenya, Dynamic changes in the structure, chemical state and catalytic selectivity of Cu nanocubes during CO 2 electroreduction: size and support effects, Angew. Chem. Int. Ed. 57 (2018) 6192–6197.
[7] R.V. Mom, L.E. Sandoval-Diaz, D. Gao, C.H. Chuang, E.A. Carbonio, T.E. Jones, R. Arrigo, D. Ivanov, M. Hävecker, B. Roldan Cuenya, R. Schlögl, T. Lunkenbein, A. Knop-Gericke, J.J. Velasco-Vélez, Assessment of the degradation mechanisms of Cu electrodes during the CO2 reduction reaction, ACS Appl. Mater. Interfaces 15 (2023) 30052–30059.
[8] P. Grosse, A. Yoon, C. Rettenmaier, A. Herzog, S.W. Chee, B. Roldan Cuenya, Dynamic transformation of cubic copper catalysts during CO2 electroreduction and its impact on catalytic selectivity, Nat. Commun. 12 (2021) 6736.
[9] B. Tomc, M. Bele, M.A. Nazrulla, P. Šket, M. Finšgar, A.K. Surca, A.R. Kamšek, M. Šala, J.Š. Hudoklin, M. Huš, B. Likozar, N. Hodnik, Deactivation of copper catalysts during CO2 reduction occurs via dissolution and selective redeposition mechanism, J. Mater. Chem. A 13 (2025) 4119–4128.
[10] J. de Ruiter, V.R.M. Benning, S. Yang, B.J. den Hartigh, H. Wang, P.T. Prins, J. M. Dorresteijn, J.C.L. Janssens, G. Manna, A.V. Petukhov, B.M. Weckhuysen, F. T. Rabouw, W. van der Stam, Multiscale X-ray scattering elucidates activation and deactivation of oxide-derived copper electrocatalysts for CO2 reduction, Nat. Commun. 16 (2025) 373.
[11] J. Huang, N. Hörmann, E. Oveisi, A. Loiudice, G.L. De Gregorio, O. Andreussi, N. Marzari, R. Buonsanti, Potential-induced nanoclustering of metallic catalysts during electrochemical CO2 reduction, Nat. Commun. 9 (2018) 3117.
[12] J. Kok, J. de Ruiter, W. van der Stam, T. Burdyny, Interrogation of oxidative pulsed methods for the stabilization of copper electrodes for CO2 electrolysis, J. Am. Chem. Soc. 146 (2024) 19509–19520.
[13] Q. Liu, Q. Jiang, L. Li, W. Yang, Spontaneous reconstruction of copper active sites during the alkaline CORR: degradation and recovery of the performance, J. Am. Chem. Soc. 146 (2024) 4242–4251.
[14] Y. Yang, J. Feijóo, M. Figueras-Valls, C. Chen, C. Shi, M.V. Fonseca Guzman, Y. Murhabazi Maombi, S. Liu, P. Jain, V. Briega-Martos, Z. Peng, Y. Shan, G. Lee, M. Rebarchik, L. Xu, C.J. Pollock, J. Jin, N.E. Soland, C. Wang, M.B. Salmeron, Z. Chen, Y. Han, M. Mavrikakis, P. Yang, Operando probing dynamic migration of copper carbonyl during electrocatalytic CO2 reduction, Nat. Catal. 8 (2025) 579–594.
[15] H. Jung, S.Y. Lee, C.W. Lee, M.K. Cho, D.H. Won, C. Kim, H.S. Oh, B.K. Min, Y. J. Hwang, Electrochemical fragmentation of Cu 2 O nanoparticles enhancing selective C-C coupling from CO 2 reduction reaction, J. Am. Chem. Soc. 141 (2019) 4624–4633.
[16] D. Zhong, D. Cheng, Q. Fang, Y. Liu, J. Li, Q. Zhao, Understanding the restructuring and degradation of oxide-derived copper during electrochemical CO2 reduction, Chem. Eng. J. 470 (2023) 143907.
[17] R. Serra-Maia, J.B. Varley, S.E. Weitzner, H. Yu, R. Shi, J. Biener, S.A. Akhade, E. A. Stach, Decoupling CO2 effects from electrochemistry: a mechanistic study of copper catalyst degradation, iScience 28 (2025) 111851, https://doi.org/10.1016/j.isci.2025.111851.
[18] D. Takamatsu, N. Fukatani, A. Yoneyama, T. Hirano, K. Hirai, S. Yabuuchi, K. Watanabe, K. Kamiya, S. Nakanishi, Dynamic relocation of copper catalysts in gas diffusion electrodes during CO2 electroreduction, J. Am. Chem. Soc. 147 (2025) 24103–24112, https://doi.org/10.1021/jacs.5c07944.
[19] S.H. Lee, J.E. Avilés Acosta, D. Lee, D.M. Larson, H. Li, J. Chen, J. Lee, E. Erdem, D. U. Lee, S.J. Blair, A. Gallo, H. Zheng, A.C. Nielander, C.J. Tassone, T.F. Jaramillo, W.S. Drisdell, Structural transformation and degradation of Cu oxide nanocatalysts during electrochemical CO2 reduction, J. Am. Chem. Soc. 147 (2025) 6536–6548.
[20] S.H. Lee, J.C. Lin, M. Farmand, A.T. Landers, J.T. Feaster, J.E. Avilés Acosta, J. W. Beeman, Y. Ye, J. Yano, A. Mehta, R.C. Davis, T.F. Jaramillo, C. Hahn, W. S. Drisdell, Oxidation state and surface reconstruction of Cu under CO2reduction conditions from in situ X-Ray characterization, J. Am. Chem. Soc. 143 (2) (2021) 588–592.
[21] S. Chen, F. Farzinpour, N. Kornienko, Dynamic active sites behind cu-based electrocatalysts: original or restructuring-induced catalytic activity, Chem 11 (2025) 102575.
[22] C. Long, X. Liu, K. Wan, Y. Jiang, P. An, C. Yang, G. Wu, W. Wang, J. Guo, L. Li, K. Pang, Q. Li, C. Cui, S. Liu, T. Tan, Z. Tang, Regulating reconstruction of oxide-derived Cu for electrochemical CO 2 reduction toward n-propanol, Sci. Adv. 9 (2023) eadi6119.
[23] B. Ligt, L.B. Donk, F.A. Rollier, J.F.M. Simons, M.C. Figueiredo, E.J.M. Hensen, Restructuring of shape-controlled Cu2O catalysts during CO2 electroreduction, J. Electroanal. Chem. 1002 (2026) 119742.
[24] O. Moradlou, M. Qorbani, A. Sabbah, V. Modak, M.E. Ashebir, O. Nasr, C.Y. Huang, F.A. Ramadani, C.H. Wang, H.L. Wu, L.C. Chen, K.H. Chen, Restricting copper reconstruction with ultrathin polydopamine for selective and stable electrochemical CO2 reduction reaction to C2 products, Adv. Energy Sustain. Res. (2025) e202500354.
[25] A. Sakamoto, A. Suzuki, A. Isobe, N. Matsumoto, R. Shang, K. Kubo, T. Mizuta, A. Kuzume, S. Kume, Surface modification via click chemistry enhances CO 2 reduction selectivity between C 2+ /C 1 on shape-controlled Cu 2 O, ChemistryEurope (2025) e202500330.
[26] J. Vavra, G.P.L. Ramona, F. Dattila, A. Kormányos, T. Priamushko, P.P. Albertini, A. Loiudice, S. Cherevko, N. Lopéz, R. Buonsanti, Solution-based Cu+ transient species mediate the reconstruction of copper electrocatalysts for CO2 reduction, Nat. Catal. 7 (2024) 89–97.
[27] Q. Zhang, Z. Song, X. Sun, Y. Liu, J. Wan, S.B. Betzler, Q. Zheng, J. Shangguan, K. C. Bustillo, P. Ercius, P. Narang, Y. Huang, H. Zheng, Atomic dynamics of electrified solid–liquid interfaces in liquid-cell TEM, Nature 630 (2024) 643–647.
[28] Q. Wu, R. Du, P. Wang, G.I.N. Waterhouse, J. Li, Y. Qiu, K. Yan, Y. Zhao, W. W. Zhao, H.J. Tsai, M.C. Chen, S.F. Hung, X. Wang, G. Chen, Nanograin-boundary-abundant Cu2O-Cu nanocubes with high C2+ selectivity and good stability during electrochemical CO2 reduction at a current density of 500 MA/Cm2, ACS Nano 17 (2023) 12884–12894, https://doi.org/10.1021/acsnano.3c04951.
[29] C. Zhang, Y. Gu, Q. Jiang, Z. Sheng, R. Feng, S. Wang, H. Zhang, Q. Xu, Z. Yuan, F. Song, Exploration of Gas-Dependent Self-Adaptive Reconstruction Behavior of Cu2O for Electrochemical CO2 Conversion to Multi-Carbon Products, Nanomicro Lett. 17 (2025) 66.
[30] Y. Hori, H. Konishi, T. Futamura, A. Murata, O. Koga, H. Sakurai, K. Oguma, Deactivation of Copper Electrode" in Electrochemical Reduction of CO2, Electrochim. Acta 50 (2005) 5354–5369.
[31] Z.Q. Liang, T.T. Zhuang, A. Seifitokaldani, J. Li, C.W. Huang, C.S. Tan, Y. Li, P. De Luna, C.T. Dinh, Y. Hu, Q. Xiao, P.L. Hsieh, Y. Wang, F. Li, R. Quintero-Bermudez, Y. Zhou, P. Chen, Y. Pang, S.C. Lo, L.J. Chen, H. Tan, Z. Xu, S. Zhao, D. Sinton, E. H. Sargent, Copper-on-Nitride Enhances the Stable Electrosynthesis of Multi-Carbon Products from CO2, Nat. Commun. 9 (2018) 3828.
[32] V. Okatenko, A. Loiudice, M.A. Newton, D.C. Stoian, A. Blokhina, A.N. Chen, K. Rossi, R. Buonsanti, Alloying as a Strategy to Boost the Stability of Copper Nanocatalysts during the Electrochemical CO2 Reduction Reaction, J. Am. Chem. Soc. 145 (2023) 5370–5383.
[33] B. Sahin, M. Kraehling, V. Facci Allegrini, J. Leung, K. Wiesner-Fleischer, E. Magori, R. Pastusiak, A. Tawil, T. Hodges, E. Brooke, E.C. Corbos, M. Fleischer, E. Simon, O. Hinrichsen, Fine-Tuned Combination of Cell and Electrode Designs Unlocks Month-Long Stable Low Temperature Cu-Based CO2 Electrolysis, J. CO2 Util. 82 (2024) 102766.
[34] B. Tomc, M. Hotko, A. Marsel, N. Maselj, M. Plut, M. Svete, L. Suhadolnik, M. Šala, M. Bele, M. Kostelec, P. Farinazzo, B. Dias Martins, D. Strmčnik, M. Gaberšček, Hodnik N. Self-Correcting Operando Impedance Spectroscopy Enables Dy-Namic Adaptability and, Self-correcting operando impedance spectroscopy enables dynamic adaptability and mechanistic insights of electrochemical CO2 reduction, ChemRxiv (2025), https://doi.org/10.26434/chemrxiv-2025-rlvth.
[35] Y. Jännsch, J.J. Leung, M. Hämmerle, E. Magori, K. Wiesner-Fleischer, E. Simon, M. Fleischer, R. Moos, Pulsed potential electrochemical CO2 reduction for enhanced stability and catalyst reactivation of copper electrodes, Electrochem. Commun. 121 (2020) 106861.
[36] A. Engelbrecht, C. Uhlig, O. Stark, M. Hämmerle, G. Schmid, E. Magori, K. Wiesner-Fleischer, M. Fleischer, R. Moos, On the Electrochemical CO 2 Reduction at Copper Sheet Electrodes with Enhanced Long-Term Stability by Pulsed Electrolysis, J. Electrochem. Soc. 165 (2018) J3059–J3068.

[37] C.A. Obasanjo, A.S. Zeraati, H.S. Shiran, T.N. Nguyen, S.M. Sadaf, M.G. Kibria, C. T. Dinh, In Situ Regeneration of Copper Catalysts for Long-Term Electrochemical CO2 Reduction to Multiple Carbon Products, J. Mater. Chem. A Mater. 10 (2022) 20059–20070.
[38] W. Lai, Z. Ma, J. Zhang, Y. Yuan, Y. Qiao, H. Huang, Dynamic Evolution of Active Sites in Electrocatalytic CO2 Reduction Reaction: Fundamental Understanding and Recent Progress, Adv. Funct. Mater. 32 (16) (2022) 2111193, https://doi.org/10.1002/adfm.202111193.
[39] N. Vorlaufer, J. Josten, A. Hutzler, C.A. Macauley, N. Martić, M. Weiser, G. Schmid, K.J.J. Mayrhofer, P. Felfer, Understanding the Degradation of Ag $_2$ Cu $_2$ O $_3$ Electrocatalysts for CO $_2$ Reduction, Nanoscale Adv. 7 (2025) 6005–6016, https://doi.org/10.1039/D5NA00328H.
[40] D. Hursán, J. Timoshenko, A. Martini, H.S. Jeon, E. Ortega, M. Rüscher, A. Bergmann, A. Yoon, U. Hejral, A. Herzog, C. Rettenmaier, F.T. Haase, P. Grosse, B. Roldan Cuenya, CO 2 Reduction on Copper-Nitrogen-Doped Carbon Catalysts Tuned by Pulsed Potential Electrolysis: Effect of Pulse Potential, Adv. Funct. Mater. (2025) e10827, https://doi.org/10.1002/adfm.202510827.
[41] M. van der Veer, N. Daems, P. Cool, T. Breugelmans, Enhancing Selectivity and Stability in Electrochemical CO2 Reduction Using Tailored Sputtered CuAg Electrodes, Green. Chem. 27 (2025) 6039–6055.
[42] W. Fang, R. Lu, F.M. Li, C. He, D. Wu, K. Yue, Y. Mao, W. Guo, B. You, F. Song, T. Yao, Z. Wang, B.Y. Xia, Low-Coordination Nanocrystalline Copper-Based Catalysts through Theory-Guided Electrochemical Restructuring for Selective CO2 Reduction to Ethylene, Angew. Chem. Int. Ed. 63 (2024) e202319936.
[43] H. Wu, L. Huang, J. Timoshenko, K. Qi, W. Wang, J. Liu, Y. Zhang, S. Yang, E. Petit, V. Flaud, J. Li, C. Salameh, P. Miele, L. Lajaunie, B. Roldán Cuenya, D. Rao, D. Voiry, Selective and Energy-Efficient Electrosynthesis of Ethylene from CO2 by Tuning the Valence of Cu Catalysts through Aryl Diazonium Functionalization, Nat. Energy 9 (2024) 422–433.
[44] F. Zhang, N. Cao, C. Wang, S. Wang, Y. He, Y. Shi, M. Yan, Y. Bao, Z. Li, P. Xie, In Situ Stabilization of Cu+ for CO2 Electroreduction via Environmental-Molecules-Induced ZnO1-x Shield, Nat. Commun. 16 (2025) 6082.
[45] M.W. Schreiber, Industrial CO2 Electroreduction to Ethylene: Main Technical Challenges, Curr. Opin. Electrochem 44 (2024) 101438.
[46] Y.L. Chung, S. Kim, Y. Lee, D.T. Wijaya, C.W. Lee, K. Jin, J. Na, Pulsed Electrolysis for CO2 Reduction: Techno-Economic Perspectives. iScience, Elsevier Inc, August 16, 2024 110383, https://doi.org/10.1016/j.isci.2024.110383.
[47] W. Xi, H. Zhou, P. Yang, H. Huang, J. Tian, M. Ratova, D. Wu, Pulse Manipulation on Cu-Based Catalysts for Electrochemical Reduction of CO2, ACS Catal. 14 (18) (2024) 13697–13722.
[48] X. Wang, M. Jiang, P. Yang, H. Zhou, W. Xi, J. Duan, M. Ratova, D. Wu, X. Jiang, Recent Advances in Pulsed Electrochemical Techniques: Synthesis of Electrode Materials and Electrocatalytic Reactions. Surfaces and Interfaces, Elsevier B.V, July 1, 2024 104519, https://doi.org/10.1016/j.surfin.2024.104519.
[49] W. Chen, Y. He, Y. Zou, S. Wang, Pulsed Electrochemistry: A Pathway to Enhanced Electrocatalysis and Sustainable Electrosynthesis, Natl. Sci. Open 3 (2024) 20240047.
[50] G. Gao, B.N. Khiarak, H. Liu, T. Trần-Phú, C.A. Obasanjo, J. Crane, H.D.T. Lai, G.T. S.T. da Silva, V. Golovanova, J. Li, H. Ze, J. Weiss, Z. Zhang, S. Lee, R.K. Hocking, F.P. García de Arquer, E.H. Sargent, C.T. Dinh, Recoverable Operation Strategy for Selective and Stable Electrochemical Carbon Dioxide Reduction to Methane, Nat. Energy (2025), https://doi.org/10.1038/s41560-025-01883-w.
[51] X.Da Zhang, T. Liu, C. Liu, D.S. Zheng, J.M. Huang, Q.W. Liu, W.W. Yuan, Y. Yin, L. R. Huang, M. Xu, Y. Li, Z.Y. Gu, Asymmetric Low-Frequency Pulsed Strategy Enables Ultralong CO2 Reduction Stability and Controllable Product Selectivity, J. Am. Chem. Soc. 145 (2023) 2195–2206.
[52] L. Xu, X. Ma, L. Wu, X. Tan, X. Song, Q. Zhu, C. Chen, Q. Qian, Z. Liu, X. Sun, S. Liu, B. Han, In Situ Periodic Regeneration of Catalyst during CO2 Electroreduction to C2+ Products, Angew. Chem. Int. Ed. 61 (37) (2022) e202210375, https://doi.org/10.1002/anie.202210375.
[53] J.Y. Huang, X.Da Zhang, H. Yang, Q.W. Liu, W.W. Yuan, W.C. Lai, Z.Y. Gu, Pulsed Strategy Steers the Structural Evolution of Cu Metal–Organic Framework for CO2 Reduction to Methane, Chem. A Eur. J. 31 (35) (2025) e202500744, https://doi.org/10.1002/chem.202500744.
[54] T.N. Nguyen, Z. Chen, A.S. Zeraati, H.S. Shiran, S.M. Sadaf, M.G. Kibria, E. H. Sargent, C.T. Dinh, Catalyst Regeneration via Chemical Oxidation Enables Long-Term Electrochemical Carbon Dioxide Reduction, J. Am. Chem. Soc. 144 (2022) 13254–13265.
[55] Y. Wu, H. Zhu, W. Wang, J. Shi, Y. Sun, F. Bai, F. Yu, Y. Wu, Y. Chen, Unlocking the Mystery of Pulse-Enhanced CO2 Electroreduction on Copper in Carbonate Media, J. Energy Chem. 107 (2025) 416–426.
[56] R. Casebolt, K. Levine, J. Suntivich, T. Hanrath, Pulse Check: Potential Opportunities in Pulsed Electrochemical CO2 Reduction, Joule 5 (2021) 1987–2026.
[57] X.K. Lu, W. Ni, A.E. Deberghes, L.C. Seitz, Insight into the Effects of Pulsed CO2 Electrolysis in a Zero-Gap Electrolyzer, Chem. Commun. 61 (2025) 9884–9887.
[58] T.N. Nguyen, Z. Chen, A.S. Zeraati, H.S. Shiran, S.M. Sadaf, M.G. Kibria, E. H. Sargent, C.T. Dinh, Catalyst Regeneration via Chemical Oxidation Enables Long-Term Electrochemical Carbon Dioxide Reduction, J. Am. Chem. Soc. 144 (29) (2022) 13254–13265, https://doi.org/10.1021/jacs.2c04081.
[59] J. Timoshenko, A. Bergmann, C. Rettenmaier, A. Herzog, R.M. Arán-Ais, H.S. Jeon, F.T. Haase, U. Hejral, P. Grosse, S. Kühl, E.M. Davis, J. Tian, O. Magnussen, B. Roldan Cuenya, Steering the Structure and Selectivity of CO2 Electroreduction Catalysts by Potential Pulses, Nat. Catal. 5 (2022) 259–267.
[60] R.M. Arán-Ais, F. Scholten, S. Kunze, R. Rizo, B. Roldan Cuenya, The Role of in Situ Generated Morphological Motifs and Cu(i) Species in C2+ Product Selectivity during CO2 Pulsed Electroreduction, Nat. Energy 5 (2020) 317–325.
[61] L.C. Tănase, M.J. Prieto, L. de Souza Caldas, A. Tiwari, F. Scholten, P. Grosse, A. Martini, J. Timoshenko, T. Schmidt, B. Roldan Cuenya, Morphological and Chemical State Effects in Pulsed CO2 Electroreduction on Cu(100) Unveiled by Correlated Spectro-Microscopy, Nat. Catal. 8 (2025) 881–890.
[62] Z. Li, L. Wang, T. Wang, L. Sun, W. Yang, Steering the Dynamics of Reaction Intermediates and Catalyst Surface during Electrochemical Pulsed CO2 Reduction for Enhanced C2+ Selectivity, J. Am. Chem. Soc. 145 (2023) 20655–20664.
[63] R. Reske, H. Mistry, F. Behafarid, B. Roldan Cuenya, P. Strasser, Particle Size Effects in the Catalytic Electroreduction of CO2 on Cu Nanoparticles, J. Am. Chem. Soc. 136 (2014) 6978–6986.
[64] G.L. De Gregorio, T. Burdyny, A. Loiudice, P. Iyengar, W.A. Smith, R. Buonsanti, Facet-Dependent Selectivity of Cu Catalysts in Electrochemical CO2 Reduction at Commercially Viable Current Densities, ACS Catal. 10 (2020) 4854–4862.
[65] O.J. Wahab, M. Kang, E. Daviddi, M. Walker, P.R. Unwin, Screening Surface Structure-Electrochemical Activity Relationships of Copper Electrodes under CO2Electroreduction Conditions, ACS Catal. 12 (2022) 6578–6588.
[66] Y. Huang, A.D. Handoko, P. Hirunsit, B.S. Yeo, Electrochemical Reduction of CO2 Using Copper Single-Crystal Surfaces: Effects of CO* Coverage on the Selective Formation of Ethylene, ACS Catal. 7 (2017) 1749–1756.
[67] S. Popovic, M. Bele, N. Hodnik, Reconstruction of Copper Nanoparticles at Electrochemical CO2 Reduction Reaction Conditions Occurs via Two-Step Dissolution/Redeposition Mechanism, ChemElectroChem 8 (2021) 2634–2639.
[68] J. Vavra, T.H. Shen, D. Stoian, V. Tileli, R. Buonsanti, Real-Time Monitoring Reveals Dissolution/Redeposition Mechanism in Copper Nanocatalysts during the Initial Stages of the CO2 Reduction Reaction, Angew. Chem. Int. Ed. 60 (2021) 1347–1354.
[69] F.D. Speck, S. Cherevko, Electrochemical Copper Dissolution: A Benchmark for Stable CO2 Reduction on Copper Electrocatalysts, Electrochem. Commun. 115 (2020) 106739.
[70] Y. Yang, S. Louisia, S. Yu, J. Jin, I. Roh, C. Chen, M.V. Fonseca Guzman, J. Feijóo, P.C. Chen, H. Wang, C.J. Pollock, X. Huang, Y.T. Shao, C. Wang, D.A. Muller, H. D. Abruña, P. Yang, Operando Studies Reveal Active Cu Nanograins for CO2 Electroreduction, Nature 614 (7947) (2023) 262–269.
[71] B. Tomc, M. Bele, M. Plut, M. Kostelec, S. Popović, M.A. Nazrulla, F. Ruiz-Zepeda, A.R. Kamšek, M. Šala, A. Elbataioui, L.D. Rafailović, Y.B. Pissolitto, F. Trivinho-Strixino, W.J. Stępniowski, L. Suhadolnik, N. Hodnik, Recognizing the Universality of Copper Reconstruction Via Dissolution–Redeposition at the Onset of CO $_2$ Reduction, J. Phys. Chem. Lett. 16 (2025) 9553–9560.
[72] D. Hochfilzer, J.E. Sørensen, E.L. Clark, S.B. Scott, I. Chorkendorff, J. Kibsgaard, The Importance of Potential Control for Accurate Studies of Electrochemical CO Reduction, ACS Energy Lett. 6 (2021) 1879–1885.
[73] S.H. Lee, J.E. Avilés Acosta, D. Lee, D.M. Larson, H. Li, J. Chen, J. Lee, E. Erdem, D. U. Lee, S.J. Blair, A. Gallo, H. Zheng, A.C. Nielander, C.J. Tassone, T.F. Jaramillo, W.S. Drisdell, Structural Transformation and Degradation of Cu Oxide Nanocatalysts during Electrochemical CO $_2$ Reduction, J. Am. Chem. Soc. 147 (2025) 6536–6548.
[74] S. Popović, M.A. Nazrulla, P. Šket, K.M. Kamal, B. Likozar, L. Suhadolnik, L. Pavko, A.K. Surca, M. Bele, N. Hodnik, Electrochemically-Grown Chloride-Free Cu2O Nanocubes Favorably Electroreduce CO2 to Methane: The Interplay of Appropriate Electrochemical Protocol, Electrochim. Acta 436 (2022) 141458.
[75] N. Hodnik, S. Cherevko, Spot the Difference at the Nanoscale: Identical Location Electron Microscopy in Electrocatalysis, Curr. Opin. Electrochem 15 (2019) 73–82.
[76] B. Tomc, M. Bele, A.R. Kamšek, M. Martins, A. Marsel, M. Hotko, S. Popović, G. Kapun, Č. Donik, M. Kostelec, M. Godec, N. Hodnik, L. Suhadolnik, Workflow and Practical Guidance for Identical Location Scanning Electron Microscopy: Reliable Tracking of Localized Transformations, Small Methods (2025) e01290.
[77] N.H. Tran, H.P. Duong, G. Rousse, S. Zanna, M.W. Schreiber, M. Fontecave, Selective Ethylene Production from CO2and CO Reduction via Engineering Membrane Electrode Assembly with Porous Dendritic Copper Oxide, ACS Appl. Mater. Interfaces 14 (2022) 31933–31941.
[78] C. Reller, R. Krause, E. Volkova, B. Schmid, S. Neubauer, A. Rucki, M. Schuster, G. Schmid, Selective Electroreduction of CO2 toward Ethylene on Nano Dendritic Copper Catalysts at High Current Density, Adv. Energy Mater. 7 (2017).
[79] Y. Yang, H. Zeng, D. Wang, Y. Wu, J. Chen, Y. Huang, P. Wang, W. Feng, Fractal Growth of Quasi Two-Dimensional Copper Dendrites by Template-Free Electrodeposition, Langmuir 39 (8) (2023) 3045–3051.
[80] J. Chen, J.J. Davies, A.S. Goodfellow, S.M.D. Hall, H.G. Lancaster, X. Liu, C. J. Rhodes, W. Zhou, Growth Mechanisms of Ag and Cu Nanodendrites via Galvanic Replacement Reactions, Progress Nat. Sci. Mater. Int. 31 (1) (2021) 141–151.
[81] D. Cheng, K.L.C. Nguyen, V. Sumaria, Z. Wei, Z. Zhang, W. Gee, Y. Li, C.G. Morales-Guio, M. Heyde, B. Roldan Cuenya, A.N. Alexandrova, P. Sautet, Structure Sensitivity and catalyst restructuring for CO2 electro-reduction on copper, Nat. Commun. 16 (1) (2025) 4064.
[82] M. Finšgar, S. Peljhan, A. Kokalj, J. Kovač, I. Milošev, Determination of the Cu2O thickness on BTAH-Inhibited copper by reconstruction of auger electron spectra, J. Electrochem. Soc. 157 (10) (2010). C295.
[83] H. Mehrabi, S.K. Conlin, T.I. Hollis, B.S. Gattis, J. Nelson Weker, R.H. Coridan, Electrochemical control of the morphology and functional properties of hierarchically structured, dendritic Cu surfaces, Energy Technol. 11 (2023) 2201124, https://doi.org/10.1002/ente.202201124.
[84] N. Rashid, M.A. Bhat, P.P. Ingole, Dendritic copper microstructured electrodeposits for efficient and selective electrochemical reduction of carbon dioxide into C1 and C2 hydrocarbons, J. CO2 Util. 38 (2020) 385–397.

[85] N.M. Schneider, J.H. Park, J.M. Grogan, D.A. Steingart, H.H. Bau, F.M. Ross, Nanoscale evolution of interface morphology during electrodeposition, Nat. Commun. 8 (1) (2017) 2174.
[86] Y. Yang, H. Zeng, D. Wang, Y. Wu, J. Chen, Y. Huang, P. Wang, W. Feng, Fractal Growth of Quasi two-dimensional copper dendrites by template-free electrodeposition, Langmuir 39 (8) (2023) 3045–3051, https://doi.org/10.1021/acs.langmuir.2c03069.
[87] T. Qin, Y. Qian, F. Zhang, A. Chen, B. Lin, Enhanced electrochemical reduction of CO2 to ethylene on electrodeposited copper in 0.1 M KHCO3, Int. J. Electrochem. Sci. 13 (11) (2018) 10101–10112, https://doi.org/10.20964/2018.11.42.
[88] P.P. Lopes, D.Y. Chung, X. Rui, H. Zheng, H. He, P.F.B.D. Martins, D. Strmcnik, V. R. Stamenkovic, P. Zapol, J.F. Mitchell, R.F. Klie, N.M. Markovic, Dynamically stable active sites from surface evolution of perovskite materials during the oxygen evolution reaction, J. Am. Chem. Soc. 143 (2021) 2741–2750.
[89] D.Y. Chung, P.P. Lopes, P. Farinazzo Bergamo Dias Martins, H. He, T. Kawaguchi, P. Zapol, H. You, D. Tripkovic, D. Strmcnik, Y. Zhu, S. Seifert, S. Lee, V. R. Stamenkovic, N.M. Markovic, Dynamic stability of active sites in Hydr(Oxy) oxides for the oxygen evolution reaction, Nat. Energy 5 (2020) 222–230.
[90] C. Thammaniphit, J. Santatiwongchai, S. Impeng, P. Khemthong, K. Meesombad, K. Faungnawakij, T. Hanrath, R. Methaapanon, P. Chakthranont, Spikes effect: decoding and redesigning pulsed electrochemical CO2reduction for enhanced C–C coupling on oxide-derived copper, ACS Catal. 15 (2025) 17003–17014.
[91] L. Wu, S. Jia, R. Wang, J. Feng, L. Zhang, H. Liu, X. Tong, R. Feng, X. Kang, Q. Zhu, Q. Qian, L. Xu, X. Sun, B. Han, Steering the catalyst structure and intermediates adsorption configuration during pulsed nitrate electroreduction, Nat. Commun. 16 (1) (2025), https://doi.org/10.1038/s41467-025-65391-x.
[92] W. Chen, Y. He, L. Xu, Y. Zou, S. Wang, H. Pang, Pulse potential modulation of Cu-based catalysts for stabilizing formaldehyde oxidation with anodic hydrogen production, Chem. Eng. J. 514 (2025), https://doi.org/10.1016/j.cej.2025.162960.
[93] N. Behera, S. Rodrigo, A. Hazra, R. Maity, L. Luo, Revisiting alternating current electrolysis for organic synthesis. Current Opinion in Electrochemistry, Elsevier B. V, February 1, 2024, https://doi.org/10.1016/j.coelec.2023.101439.
[94] B. Tomc, M. Hotko, A. Marsel, N. Maselj, M. Svete, L. Suhadolnik, M. Bele, P. Farinazzo Bergamo Dias Martins, D. Strmčnik, M. Gaberšček, N. Hodnik, Operando impedance spectroscopy informed dynamic internal resistance compensation mitigates bubble-induced distortions of the applied potential, ACS Electrochem 1 (2025) 2823–2830.